



THE UNIVERSITY *of* EDINBURGH
**School of Physics
and Astronomy**

Development of an Active Deuterium Target for Dibaryon Studies

MPhys Project Report

Jake Watson

27th March, 2017

Abstract

The abstract is a short concise outline of your project area, of no more than 100 words. Avoid equations and references in an abstract.

**Supervisors: Dr. Mikhail Bashkanov, Dr. Nicholas
Zachariou**

Acknowledgements

Contents

| | |
|--|----|
| Introduction and Motivations..... | 1 |
| 1.1 Introduction | 1 |
| 1.2 Nature of the Project | 2 |
| 1.3 Project Motivations | 3 |
| Search for Dibaryons and the Crystal Ball Detector | 5 |
| 2.1 Quarks and Colour..... | 5 |
| 2.2 Exotic Hadrons | 7 |
| 2.3 Search for Dibaryons..... | 7 |
| 2.3.1 H-Dibaryon | 8 |
| 2.3.2 d'-Dibaryon | 8 |
| 2.3.3 Inevitable Dibaryon..... | 8 |
| 2.4 The ABC effect and the $d^*(2380)$ | 9 |
| 2.4.1 Open questions on the d^* | 10 |
| 2.5 d^* Studies and the Crystal Ball | 10 |
| 2.5.1 The Crystal Ball detector..... | 11 |
| Target Simulation and Design..... | 12 |
| 3.1 Target Design | 12 |
| 3.1.1 Target Description | 13 |
| 3.1.2 Measurement..... | 14 |
| 3.1.3 Geometry Justification | 14 |
| 3.1.4 Scintillator Thickness Variation..... | 15 |
| 3.2 Monte Carlo Methods | 16 |
| 3.3 Geant4 (GEometry ANd Transport)..... | 17 |
| 3.3.1 Simulation Structure | 18 |
| 3.3.2 Class List | 18 |

| | | |
|-------|--|----|
| 3.3.3 | Simulation Input | 20 |
| 3.4 | Input Energy Calculations | 21 |
| 3.4.1 | Deuteron Input Simulation..... | 21 |
| 3.4.2 | Proton Input Simulation | 25 |
| 3.5 | Simulation Parameters..... | 28 |
| 3.5.1 | Computing Resources..... | 28 |
| 3.5.2 | Source Code | 28 |
| | Simulation Results and Analysis | 29 |
| 4.1 | Data Structure..... | 29 |
| 4.2 | Stopping Cases..... | 30 |
| 4.3 | Total Background and Signal..... | 33 |
| 4.3.1 | Signal to Background | 35 |
| 4.3.2 | SBR Variation with Incident Energy | 36 |
| | Conclusions..... | 37 |
| 4.4 | Outlook | 38 |
| | References..... | 39 |

Chapter 1

Introduction and Motivations

This chapter introduces the discovery of the new d^* dibaryon, and outlines the scope of this project. This is followed by a summary of the motivations for this study.

1.1 Introduction

In 2013, a new particle was discovered which could represent a new understanding of the theory of the strong interaction – Quantum Chromodynamics. This particle is known as the $d^*(2380)$ dibaryon [1].

The world around us is made of atoms, which at their core are made up of protons and neutrons. These two particles are examples of a wider set of particles, known as the baryons, which are composed of three quarks. Together with another set known as the mesons, made up of a quark and an antiquark, they make up the vast majority of the mass that we see around us.

CHAPTER 1. INTRODUCTION AND MOTIVATIONS

Our understanding of these particles is provided by the theory of Quantum Chromodynamics, which governs any particle composed of quarks. However, there is nothing in this theory that dictates that these are the only two types of particles that can be made from quarks – many more types have been postulated to exist.

None of these theorised particles had been seen, until the discovery of this new dibaryon – a particle composed of six quarks. The full study of the nature of this particle is absolutely necessary to further our understanding of the theory of QCD.

This leads us to the goal of this project: to lay the groundwork for such study of the new dibaryon.

1.2 Nature of the Project

This project aimed to design and produce an active target, for use in the Crystal Ball detector at the MAMI Microtron facility in Mainz. This target was to be optimised for the study of the new dibaryon. This task was split into two main sections:

1. The first, and largest, section of the project was to use computer simulations, built with the Geant4 [2] simulation toolkit, to find the optimum dimensions of the new target.
2. The second section would be to build this target in the laboratory, and perform experiments on it in order to validate the results of the simulation. Due to time constraints this section was not achieved.

CHAPTER 1. INTRODUCTION AND MOTIVATIONS

Although the second section could not be completed, completion of the first section allowed me to draw all necessary conclusions to fulfil the aims of the project.

This target, composed of deuterated plastic and scintillator, should be placed in the high-intensity gamma-ray beam of 570 MeV, produced by the MAMI C accelerator. The Crystal Ball detector would then be used to detect scintillation photons originating from the interaction of the beam with the target, so as to measure the d^* decay.

The main difficulty in designing the target was the condition that any background produced was easily identified and separated, leaving only the signal from the reaction of interest. To this end, the target design was simulated using Geant4 for several different dimensions. The dimensions that resulted in the smallest background would then be chosen as the dimensions of the new prototype target. Alongside this, the simulations allowed me to predict the level of background to be expected in the real experiment.

If time had allowed, the target would have been fabricated according to the dimensions found in the previous section. This prototype would then have been tested using ambient radiation to validate the results of the simulation.

1.3 Project Motivations

There are several motivations for the project:

Firstly, and I feel the most important, a fuller understanding of QCD is possible by probing the nature of the dibaryon. If you ask any undergraduate physics student around the world what types of hadron exist, they will answer only mesons and baryons. This is now known to be incorrect. Such a

CHAPTER 1. INTRODUCTION AND MOTIVATIONS

fundamental theory must be understood fully if we are to advance our knowledge of nuclear physics.

The exact nature of the dibaryon has implications for neutron star dynamics, and other dense matter systems. If dibaryons are stable in nuclei, then two nucleons could be packed into a dibaryon with a similar radius to a single nucleon. This would make it possible to fit far more mass into the same volume. This has implications for the equation of state for such dense matter, and therefore a full understanding of the physical structure and properties of the dibaryon are required.

Chapter 2

Search for Dibaryons and the Crystal Ball Detector

This chapter introduces the theory of multi-quark states beyond baryons and mesons, and in particular the theory of the dibaryon. The method by which the $d^*(2380)$ dibaryon was discovered is outlined. Finally, the Crystal Ball detector at the MAMI Microtron facility and its use in studying the dibaryon is described.

2.1 Quarks and Colour

For over a century we have known that matter is made up of atoms, which themselves are made up of electrons orbiting a nucleus. Since the 1930s we have known that this nucleus is composed of protons and neutrons. Yet even under the constant repulsion between the protons, the nucleus survives. From this picture, we have deduced the existence of a strongly

CHAPTER 2. SEARCH FOR DIBARYONS AND THE CRYSTAL BALL DETECTOR

attractive force between the protons and neutrons, that holds the nucleus together.

In 1947, with the discovery of the pion, this picture became more complex – it marked the start of an explosion in the number of known subatomic particles. The search for order in this chaos led Gell-Mann to introduce the quark model [3].

In this view, the pion, proton and neutron are nothing more than the lightest of a range of ‘hadrons’, or particles which respond to the strong force. This is because they are not indivisible particles, but composite systems of ‘quarks’.

From here, the strong force becomes like electromagnetism, an interaction between charges. However, this new charge has subtle differences to the electrical charge. It is called ‘colour charge’, and can be one of three distinct colours. Unlike colours attract, so that three quarks charged with different colours can combine, while a fourth quark would be repelled by a quark of the same colour in the cluster of three. In addition to this picture of three-quark states, there can be systems composed of a quark and an antiquark, which will have opposite colours.

Both of these systems obey one of the fundamental principles of Quantum Chromodynamics (QCD), that such quark systems must be ‘colourless’ – the addition of the two or three different colours present in the system must produce ‘white’, in the same way that combining red, green and blue light produces white light.

Thus we have the two states of hadronic systems – the baryon, composed of three quarks, and the meson, composed of a quark and an antiquark.

CHAPTER 2. SEARCH FOR DIBARYONS AND THE CRYSTAL BALL DETECTOR

2.2 Exotic Hadrons

Now that we have understood the nature of the baryon and the meson, we might imagine that our understanding of QCD is complete. Indeed, no other hadronic state not belonging to one of these two categories has been observed (until now). Yet there is nothing in this theory which states that more complex systems are impossible.

The existence of these exotic states has been theorised since the invention of QCD, with Gell-Mann postulating the existence of pentaquarks in his original 1964 paper [3], or predicting the existence of glueballs as gluon bound states with no quark content [4]. In addition, quark/gluon hybrids, tetraquarks [5], pentaquarks [6], and finally dibaryons [7], with six quarks, have been proposed. The search for these states and others has been exhaustive [8] [9], but has yielded little.

2.3 Search for Dibaryons

The first paper on two-baryon systems appeared in 1964, by Dyson and Xuong [10]. This paper introduced dibaryons as being composed of six quarks. This was a step up from the dibaryon predictions arising from the purely phenomenological ‘Eightfold Way’ [11], and allowed new dibaryon candidates to be constructed in a more systematic manner.

This led to many more predictions of dibaryons based on the quark model, with the 1976 Jaffe paper [7] in particular kicking off a series of theoretical predictions and experimental

CHAPTER 2. SEARCH FOR DIBARYONS AND THE CRYSTAL BALL DETECTOR

detection claims. Some of the most important and credible predictions are listed below.

2.3.1 H-Dibaryon

This type of dibaryon was predicted to have an *udsuds* quark structure, and represents a bound state of two Λ baryons. It was originally predicted by Jaffe in 1976 [7], with a mass of 2150 MeV. This dibaryon prediction is the most widely cited.

2.3.2 d'-Dibaryon

This dibaryon was introduced to describe double charge exchange reactions [12]. It was predicted to decay only via the $NN\pi$ channel. The claimed mass was 2065 MeV, although this claim of detection was later withdrawn.

2.3.3 Inevitable Dibaryon

This type of dibaryon was predicted to be composed of two delta baryons [13] – a delta baryon is composed of only up or down quarks, such as *uud* or *ddd*. This dibaryon has been used to explain the so-called ‘ABC effect’. This is detailed in the next section.

CHAPTER 2. SEARCH FOR DIBARYONS AND THE CRYSTAL BALL DETECTOR

2.4 The ABC effect and the $d^*(2380)$

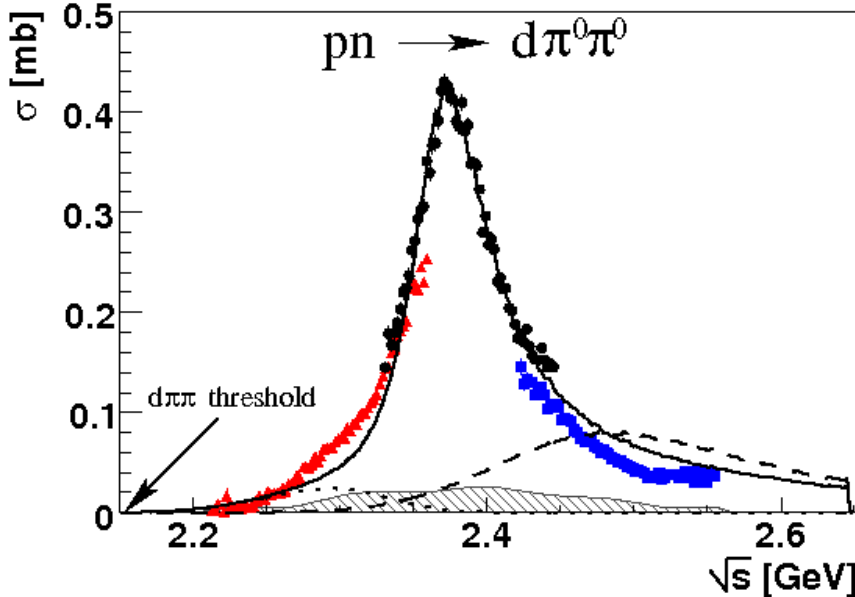


Figure 2.1: Total cross-section against CMS energy for the $pn \rightarrow d\pi^0\pi^0$ reaction. [22]

The ABC effect was first observed by Abashian, Booth and Crowe in 1960 [14], as a low-mass enhancement in the mass-invariant $\pi\pi$ production.

In 2011, a resonance was found in the production of neutral pion pairs, shown in Figure 2.1. This structure can only be attributed to the ABC effect, as other known, conventional resonances at this energy range – shown in the dashed grey and black lines – cannot explain this structure.

The ABC effect has been explicitly tied to the existence of the d^* dibaryon, as shown by Bashkanov, Clement and Skorodko [1]. Therefore, the observation of this resonance led to the assumption of the existence of a new dibaryon called the d^* , with a mass of 2380 MeV and a width of 80 MeV.

CHAPTER 2. SEARCH FOR DIBARYONS AND THE CRYSTAL BALL DETECTOR

2.4.1 Open questions on the d*

Although the existence of the d* has now been established, there remain questions to be answered. The most interesting question is on its internal structure. There are two possibilities [15]:

- The dibaryon is a bound state of two delta baryons, also known as the deltaron.
- The second possibility is that the dibaryon is a genuine six-quark state, with every quark in a single bag – also known as a hexaquark.

To answer questions like these, the dibaryon must be further probed. This leads to the reason for this project – to lay the groundwork for any future attempt to study the d* directly.

2.5 d* Studies and the Crystal Ball

To further study the dibaryon, the $d^* \rightarrow de^+e^-$ Dalitz decay should be measured. This would allow us to deduce the charge distribution and thus the size of the d*. By finding the size of the d*, we can start to comment on its likely internal structure. To measure this decay, we can reverse the above reaction and use photoexcitation [15]:

$$\gamma + d \rightarrow d^* \rightarrow d\pi^0\pi^0 \quad 1$$

This requires a photon beam energy of 500 - 600 MeV. For this project, the Crystal Ball detector at MAMI was chosen, as it can produce a high-quality beam of energies up to 1.65 GeV, and is equipped with a high-acceptance detector.

CHAPTER 2. SEARCH FOR DIBARYONS AND THE CRYSTAL BALL DETECTOR

2.5.1 The Crystal Ball detector

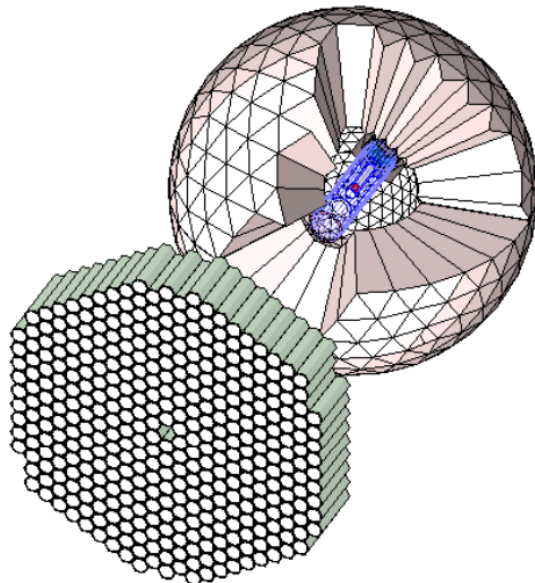


Figure 2.1: A schematic of the TAPS/Crystal Ball detector setup.

The Crystal Ball detector is based at the MAMI Microtron facility in Mainz. It consists of 672 prism-shaped NaI scintillators, of length 41cm, arranged to form a sphere as shown in Figure 2.2 Attached to the end of each of these prisms is a photo-multiplier tube. This style of detector is known as a 4π detector, as it covers almost all (94%) of the 4π -steradian solid angle around the target.

The TAPS calorimeter covers the forward angle region ($\pm 20^\circ$) not covered by the Crystal Ball, and is composed of 510 hexagonal BaF₂ scintillators. [16]

The target designed in this project would then be placed in the centre of this sphere, and exposed to the gamma-ray beam. The next chapter details the design and simulation of this target.

Chapter 3

Target Simulation and Design

This chapter details the design and use of Geant4 [2] in simulating the active target. The first half of this chapter describes the design and geometry of the target. The second half describes the nature of Geant4 and of the simulations used in this project.

3.1 Target Design

The primary task of this project was to determine the optimum dimensions of a target to study the d^* dibaryon, through measuring the deuteron scattering reaction outlined in previous sections. This was done by simulating various scintillator thicknesses in the target.

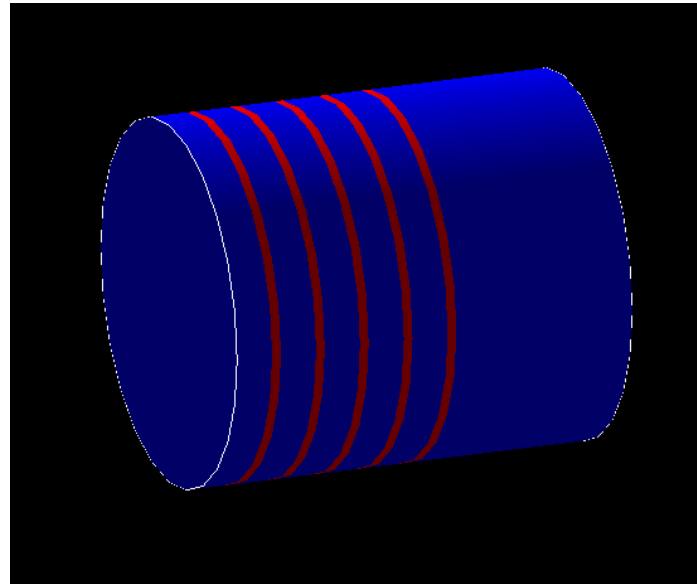


Figure 3.1: A visualisation of the target. Deuterated layers are shown as red, and scintillator is shown as blue.

3.1.1 Target Description

This project simulates a cylindrical target, composed of alternating layers of CD_2 deuterated plastic and vinyltoluene plastic scintillator.

As can be seen in Figure 3.1, there are five composite layers made up of 1 layer of CD_2 , and 1 layer of vinyltoluene, with an additional four layers of vinyltoluene at the back of the target and a single layer of vinyltoluene at the front. These extra layers of scintillator are added so that ambient background can be identified and removed.

The radius of this target is 2 cm, and the thicknesses of each CD_2 layer are 1mm (This thickness was chosen because the laboratory had it in stock, and because it is not too thick as to become opaque to the beam). The layers of vinyltoluene are varied from 1mm to 4mm, in 1mm increments.

CHAPTER 3. TARGET SIMULATION AND DESIGN

3.1.2 Measurement

To measure the signal produced by the target, several fibre-optic guides would be attached to the outside edge of each scintillator layer. These guides would lead light, produced by reaction products in the scintillator layers, to photo-multiplier tubes, to be converted into an electrical signal that could be logged.

Using coincidence testing, and exploiting the fast scintillation time of the plastic scintillator, it would be possible to identify different reaction products, that deposit energy in different layers of the target, but originate from the same particular reaction. The ability to distinguish reaction products from different reactions would be necessary for full reconstruction of events.

3.1.3 Geometry Justification

Any potential target geometry must produce a signal that can be easily separated from any background. The particular reaction to be measured was the deuteron scattering by the gamma-ray beam. However, the quasi-free reaction produces protons with energies very close to the target reaction. A full description of both of these reactions can be found in Section x.

These energies are very low, on the order of 10 MeV, so unless the thickness of the layer of production is very small neither the signal nor the background reaction products would escape the layer, and nothing could be measured. Therefore, a thin deuterated layer was necessary.

In addition, these low energies required the target to be ‘active’: the target had to, through the use of scintillators in its design, ‘amplify’ these low energy products so that they could be measured. In effect, the target becomes both the

CHAPTER 3. TARGET SIMULATION AND DESIGN

production and detection medium. With a thin deuterated plastic layer, the overall cross-section with the gamma-ray beam would be too small to produce a meaningful number of signal events. Therefore, I ‘sandwiched’ a number of thin CD₂ layers in the target, separated by scintillator layers, so as to give a significant combined cross-section with the gamma-ray beam.

To illustrate the need for this design, imagine a proton and deuteron produced in the same layer of the target, with the same energy. As they progress through the target, they will deposit energy in each layer of scintillator – however, due to the mass difference between the two particles, the rate of deposition per unit length will be different.

Therefore, the total amount deposited by each particle per layer will be different. This difference in measured deposition energy makes it possible to apply energy cuts to the resultant data, and so isolate the deuteron scattering signal from the proton production and general photon background.

3.1.4 Scintillator Thickness Variation

The most important dimension in the target design was the thickness of the scintillator layers. If the scintillator layers were too thick, all reaction products would stop within the first or second composite layer, making it impossible to distinguish signal from background. If too thin, the energy deposited in each scintillator layer would be too small to measure.

The task was then to choose a thickness of scintillator that allowed the reaction products to traverse several layers of the target before stopping, while depositing significant levels of energy. A target with this design should then produce a

CHAPTER 3. TARGET SIMULATION AND DESIGN

deuteron scattering signal that is clearly distinguishable from any background.

3.2 Monte Carlo Methods

Geant4 uses Monte Carlo methods to simulate the path of particles through matter. The nature of the processes involved at the particle level, described by quantum mechanics, dictates that the simulation cannot be purely deterministic, and must instead use randomness and probabilities to model an interaction.

The process of a Monte Carlo simulation involves repeated sampling of pseudo-random numbers, to determine the behaviour or property of some variable or phenomenon. To this end, a Monte Carlo simulation must have a source of high-quality random numbers. Because a Monte Carlo simulated process is probabilistic, the accuracy of the final result is improved by using a very large sample.

An example particle track is shown in Figure 3.2. In Geant4, the user defines a detector geometry. Any geometry must fully describe all of the properties of the system to be simulated, including object positions, shapes, dimensions, and materials.

Once a particle enters the geometry, the particle is tracked until it either leaves the geometry or is absorbed. The particle is moved through the geometry in a series of steps. At each new step, the particle has a probability of undergoing an event. For example, an incoming particle may scatter off a target particle, be absorbed, or decay. The particular type of event that occurs at each step is decided by sampling a random number. [17]

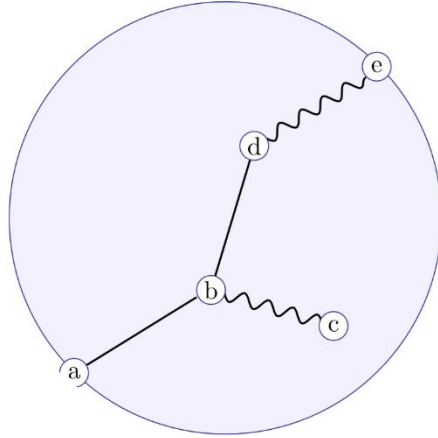


Figure 3.2: a) Incident Particle; b) Particle scattering and gamma emission; c) Gamma absorption; d) Particle absorption and gamma emission; e) Gamma escapes. [17]

The primary objective of this simulation was to simulate the interaction of a gamma-ray beam in the active target. After simulating the tracks of a large number of gamma-rays (10^6), along with deuterons and protons, the results provide a good approximation to reality.

3.3 Geant4 (GEometry ANd Transport)

Geant4 is a software toolkit used to simulate the interaction of particles in matter, and is used in fields as varied as medical imaging, nuclear physics and space technology [2]. Based on a mix of theoretical models and experimental data, Geant4's Monte Carlo simulation codes are taken to be extremely accurate.

Alongside this, Geant4 also boasts an enormous range of physical processes available for simulation, making it incredibly versatile. Once the use of Geant4 is understood, it is far quicker to design and write a simulation when compared

CHAPTER 3. TARGET SIMULATION AND DESIGN

to starting from scratch. This made it the natural choice for simulating the new active target.

3.3.1 Simulation Structure

A Geant4 simulation is built as several C++ classes. The user must define the geometry of the target, and specify which type of input particles, as well as their energy, direction of travel, and position of origin, to use. The physical processes that affect the progression of the particle through the materials of the target specified, by using structures known as ‘physics lists’ – only those processes included in the simulation’s physics list are modelled. For example, if the electromagnetic interaction is not included in the list, then the simulation will proceed as if this interaction does not exist.

The authors of Geant4 provide ready-made physics lists tailored to specific families of particles, or energy ranges. The specific physics list used in this simulation is the FTFP-BERT physics list. The models of hadronic interaction used in this list are valid up to approximately 10 GeV interaction energy, which matches the energy ranges of interest to this project. Some of the processes defined in this physics list included: electromagnetic physics; decays; hadronic elastic scattering; and hadronic interactions. These processes are all integral to the successful modelling of the interaction of deuterons in the target with the gamma-ray beam.

3.3.2 Class List

The following classes make up the simulation of the active target:

PrimaryGeneratorAction: This class defines the particle type, energy, starting position and direction of the initial particles in the simulation. Three different PrimaryGeneratorAction classes are used in this project. The

CHAPTER 3. TARGET SIMULATION AND DESIGN

first models the gamma-ray beam used in the experiment, composed of 570 MeV gamma-ray photons with direction normal to the centre of the target face. No variation in beam energy or direction is included, and photons always start from the same position.

The second models the scattered deuterons produced by interaction of the gamma-rays with the deuterium in the target. These deuterons are created randomly, with a uniform distribution, in any of the deuterated layers within the target. They have energy and direction assigned randomly, with a distribution in accordance with the kinematics of this scattering reaction.

The third models the protons produced through quasi-free production of neutrons within the deuteron. These protons are also produced randomly, with a uniform distribution, in any of the deuterated layers within the target. Their energy and momentum are randomly chosen in accordance with the kinematics of this reaction.

DetectorConstruction: This class defines the geometry and material composition of the target. The target is cylindrical, and made up of 5 composite layers of deuterated plastic of 1mm thickness, and scintillator layers of thickness varying between 1mm and 4mm. A single layer of scintillator is placed at the ‘beam-end’ of these composite layers, with 4 more layers of scintillator at the back end. The materials chosen for the target were CD₂ deuterated plastic, and vinyltoluene plastic scintillator.

In addition to defining the geometry and materials, the function *ConstructSDandField()* defines a ‘sensitive detector’ in each layer of the target. Any volume labelled as a sensitive detector automatically stores information about any particle

CHAPTER 3. TARGET SIMULATION AND DESIGN

that is incident upon it, including the energy deposited in that volume. This information is stored in a ‘*HitsCollection*’ object, which can then be accessed by the *EventAction* class.

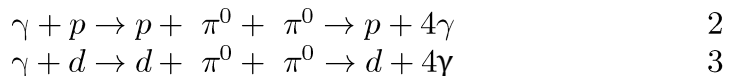
RunAction: This class is called at the beginning and end of a run. A run is a collection of events, each event consisting of 1 input particle. This class defines the format of the output file. For this simulation, the output file format is the ROOT format, allowing the simulation data to be analysed using a ROOT script.

EventAction: This class is called at the end of each event. The function *EndOfEventAction()* accesses the *HitsCollection* object created by the *DetectorConstruction* class, reads it for information about particle interactions in the target, and stores this information in the output file.

ActionInitialization: This class is called when starting the simulation application. It uses ‘user actions’ to implement the *PrimaryGenerationAction*, *DetectorConstruction*, and *EventAction* classes.

3.3.3 Simulation Input

The gamma-ray beam produced at the MAMI Microtron produces showers of secondary particles when it interacts with the target. Of all the reaction channels contributing to these showers, only two routinely produce particles in the energy range of the d* decay. [15]



Although simulating the interaction of the gamma-ray beam with the target would include these reactions, their cross-sections are very small when compared to the cumulative cross-section of all other possible reactions in the target.

CHAPTER 3. TARGET SIMULATION AND DESIGN

Because of this, only a tiny fraction of the data produced in this simulation would be due to these two reactions, and so no conclusions could be drawn about our ability to distinguish the reaction products of these two reactions from the general photon-shower background.

To overcome this problem, the products of these reactions were simulated directly. In addition to the gamma-ray input simulation, two separate simulations using either protons or deuterons as the sole input particle were designed.

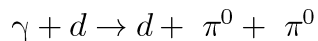
These particles were randomly assigned energies determined by either a photo-scattering kinematic calculation, or a quasi-free production calculation. Both of these calculations are outlined in the next section. Using these two separate simulations, I could generate large enough data sets to be able to draw meaningful conclusions about the distinguishability of the products of these reactions.

3.4 Input Energy Calculations

For both deuteron and proton input simulations, the input particle energy had to be scattered along a distribution determined using a photo-scattering kinematic calculation for the deuteron and a quasi-free production calculation for the proton. The details of these calculations are shown below.

3.4.1 Deuteron Input Simulation

The scattering angle/energy relation of the scattered deuterons for the below reaction is derived.



4

CHAPTER 3. TARGET SIMULATION AND DESIGN

The two pions are assumed to travel with almost identical directions in the lab frame, allowing the approximation of the two pions, in the lab frame, as a single particle of double the pion mass. This approximation reduces the problems' complexity to simple two-body kinematics. This assumption is only valid for the d^* decay to two pions.

The four vectors of the initial and final states of this interaction are shown below. The deuteron is assumed to be at rest.

Initial State:

$$p_\gamma^\mu = \begin{bmatrix} E_\gamma \\ n_\gamma \end{bmatrix}, \quad p_{di}^\mu = \begin{bmatrix} cm_d \\ 0 \end{bmatrix} \quad 5$$

Final State:

$$p_{df}^\mu = \begin{bmatrix} E_d \\ c \\ n_d \end{bmatrix}, \quad p_\pi^\mu = \begin{bmatrix} E_\pi \\ n_\pi \end{bmatrix} \quad 6$$

Where p_γ^μ is the 4-momentum of the incident photon, p_{di}^μ is the 4-momentum of the deuteron at rest, p_{df}^μ is the 4-momentum of the scattered deuteron, p_π^μ is the 4-momentum of the double-pion, E_γ is the photon energy, n_γ is the photon 3-momentum, m_d is the deuteron mass, E_d is the scattered deuteron energy, n_d is the 3-momentum of the scattered deuteron, E_π is the energy of the double-pion and n_π is the 3-momentum of the double-pion.

Using conservation of 4-momentum:

$$p_\gamma^\mu + p_{di}^\mu = p_{df}^\mu + p_\pi^\mu \quad 7$$

And rearranging to give:

$$p_\pi^\mu = p_\gamma^\mu + p_{di}^\mu - p_{df}^\mu \quad 8$$

CHAPTER 3. TARGET SIMULATION AND DESIGN

Squaring both sides of this equation gives:

$$p_\gamma^\mu p_{\mu\pi} = (p_\gamma^\mu + p_{di}^\mu - p_{df}^\mu)(p_{\mu\gamma} + p_{\mu di} - p_{\mu df}) \quad 9$$

And rearranging:

$$m_\pi^2 c^2 = 0 + 2m_d^2 c^2 + 2p_\gamma^\mu p_{\mu di} - 2p_{di}^\mu p_{\mu df} - 2p_\gamma^\mu p_{\mu df} \quad 10$$

Substituting in the 4-vectors and rearranging gives:

$$m_d^2 c^2 + E_\gamma m_d - \frac{m_\pi^2 c^2}{2} = E_d m_d + E_d \frac{E_\gamma}{c^2} - \frac{E_\gamma}{c} \cos \theta \sqrt{\frac{E_d^2}{c^2} - m_d^2 c^2 \cos^2 \theta} \quad 11$$

Where θ is the angle between the beam direction and the scattering direction. This is plotted in Figure 3.3.

For the deuteron simulation, the initial particle energies are chosen by drawing at random from the allowed range of

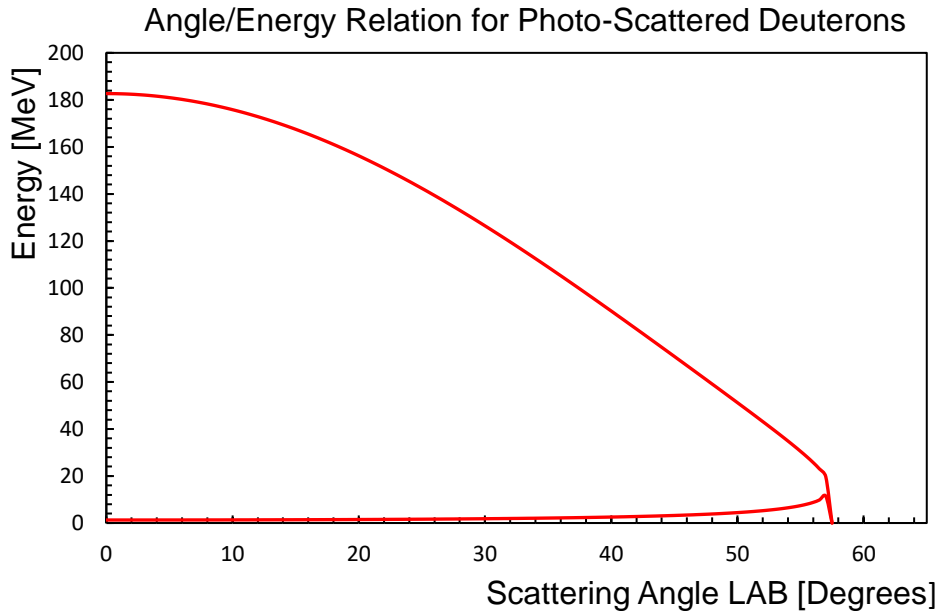


Figure 3.3: A plot of the kinetic energy of a photo-scattered deuteron versus scattering angle. The energy of the incident photon is 570 MeV.

CHAPTER 3. TARGET SIMULATION AND DESIGN

scattering angles, and substituting the selected angle into the angle/energy relation. Another random number is drawn to determine which ‘arm’ of the distribution the deuteron is scattered on. A third number is then drawn to determine which layer of deuterated material the deuteron will be created in. The deuteron is then given a ϕ component, drawn from a uniform distribution, to complete its direction vector. It is then tracked through the target. A visualisation of the simulation for this input is shown in Figure 3.4.

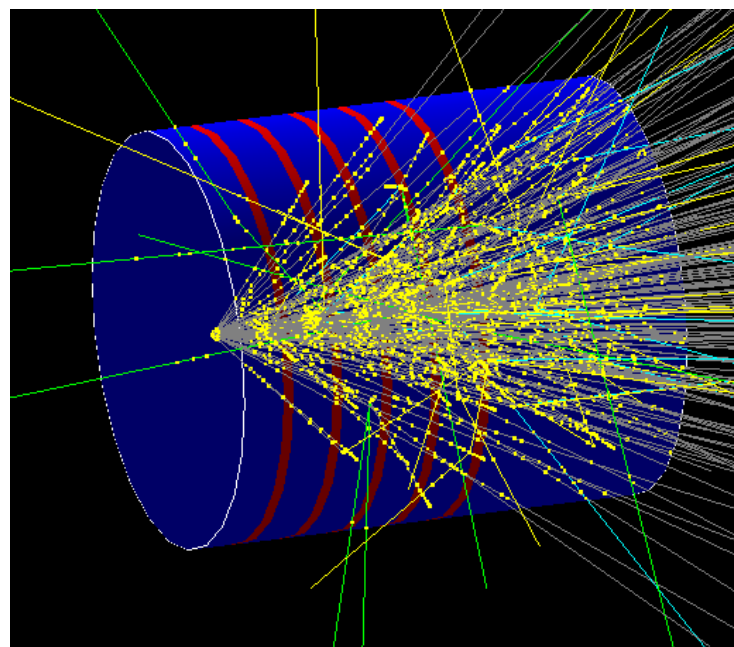


Figure 3.4: A visualisation of the simulation for the deuteron input. Grey lines represent deuteron tracks.

3.4.2 Proton Input Simulation

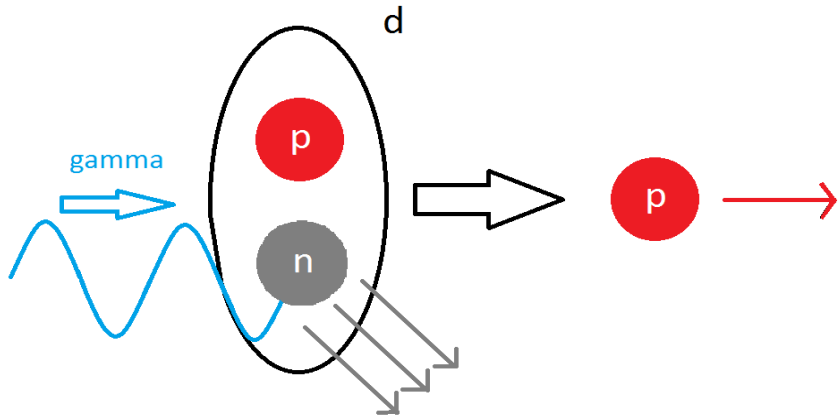


Figure 3.5: Schematic of the quasi-free production of protons on the deuteron.

The proton input simulation aims to simulate the tracks of protons produced in the following reaction:



This process is known as quasi-free production of the neutron. The de Broglie wavelength of the incident 570 MeV gamma-ray is calculated to be 2.18 fm, which is much smaller than the diameter of the deuteron, which is known to be 4.31 fm [18].

As the de Broglie wavelength of the gamma-ray is small compared to the size of the deuteron, it is much more likely to interact with the constituents of the deuteron individually. If the gamma-ray interacts with the proton, then the proton will scatter, and be detected in the scintillators of the Crystal Ball detector. However, due to the high energy of the initial gamma-ray, these protons will have a high energy and can be easily distinguished and discarded.

CHAPTER 3. TARGET SIMULATION AND DESIGN

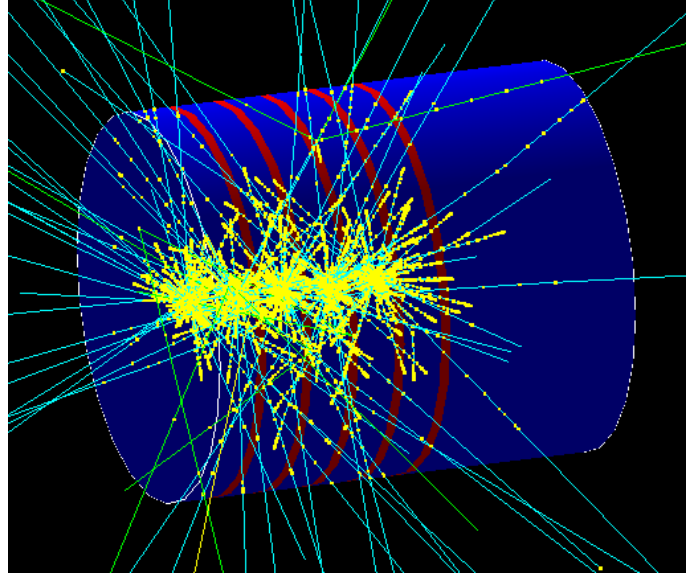


Figure 3.6: A visualisation of the simulation for the proton input. Blue lines represent proton tracks.

If the gamma-ray instead interacts with the neutron, then the neutron will scatter, leaving behind the proton. The proton's energy will be independent of the energy of the gamma-ray, and within the energy range of the d^* dibaryon decay, making this reaction the main source of background in the d^* decay range. This make it the most important reaction to simulate.

The ejection angle and energy are independent for these protons. The protons have a $\sin(\theta)$ distribution in direction, where the z-axis is normal to and into the face of the target.

CHAPTER 3. TARGET SIMULATION AND DESIGN

The distribution of Fermi energies for the protons can be found through a quantum mechanical treatment of the interaction, and depends solely on the deuteron wavefunction. The distribution is described by the Equation 13.

$$P(n_p) = \left(\frac{\frac{n_p(0.26^2 - 0.0456^2)}{(n_p^2 + 0.0456^2)}}{n_p^2 + 0.26^2} \right)^2 \quad 13$$

Where $P(n_p)$ is the probability of a proton having momentum n_p . This is based on the Hulthen wave-function for nucleons [19]. This is plotted in Figure 3.7.

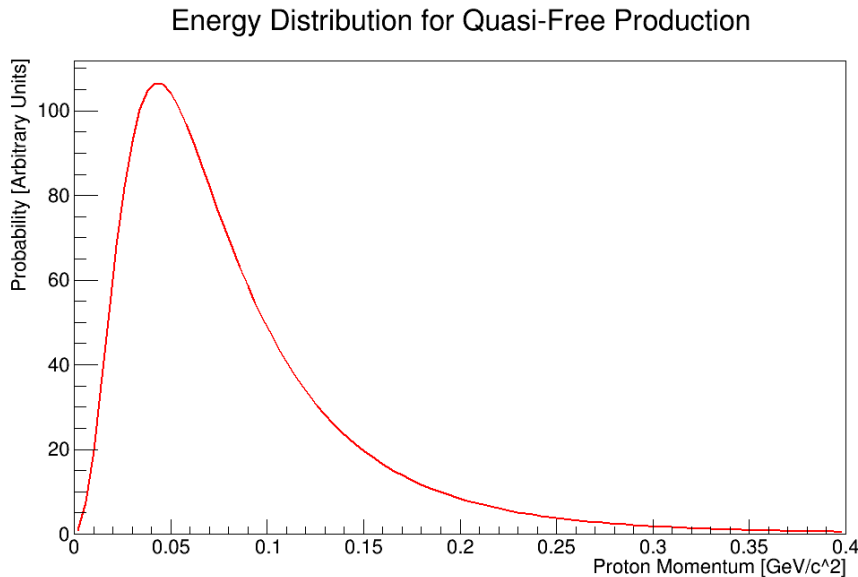


Figure 3.7: This plot shows the energy distribution of protons produced through quasi-free production of neutrons on the deuteron, for a 570 MeV incident gamma-ray.

To simulate this process in Geant4, an energy is drawn from the distribution shown above, and assigned to a proton. This proton also receives a random angle drawn from a $\sin(\theta)$ distribution, and is then tracked through the target, as shown in Figure 3.6.

3.5 Simulation Parameters

To obtain data, the simulations were run for 1 million events for each input case – photon, proton and deuteron. This was done for each of the four thicknesses of scintillator, and the results were analysed using a ROOT script. This analysis will be detailed in the next chapter. Barring choosing the input type and the scintillator thickness, no other variables were changed between simulations.

3.5.1 Computing Resources

All of the simulations were run on my own laptop: a Lenovo ThinkPad T430. This machine runs Microsoft Windows 10. It uses an Intel Core i5-3210M CPU at 2.5 GHz (2 cores, x64 bit), with 8GB of RAM. The approximate time required per simulation varied, but all were completed in under 2 hours.

The fact that such complex simulations are possible on a laptop in less than 2 hours is impressive, and is a testament to the design and optimization effort that went into Geant4.

3.5.2 Source Code

All of the source code for these simulations is available from GitHub. Please follow this link.

Insert Link Here.

Chapter 4

Simulation Results and Analysis

This chapter details the use of ROOT in analysing the data produced by the simulation of the active target, for each of the three different inputs. From this analysis, a conclusion is drawn as to the optimum target dimension to ensure signal and background separability.

4.1 Data Structure

The data from the simulations was stored in ROOT files. This format allows us to use the ROOT program to analyse them. [20] This program allows us to quickly analyse and visualise large data sets, and is provided for free by CERN.

The particular data structure used in this project was the Tree data structure. This is in effect a giant table. Every row of the table represents an event, with each column storing a different variable. A sample row is shown in Table 4.1.

CHAPTER 4. SIMULATION RESULTS AND ANALYSIS

Table 4.1: A sample row from the simulation output files.

| Incident Angle | Incident Energy | Layer 0 E-Dep | Layer 1 E-Dep | ... | Layer N E-Dep |
|----------------|-----------------|---------------|---------------|-----|---------------|
|----------------|-----------------|---------------|---------------|-----|---------------|

The simulation stores several different quantities per event, as shown in the sample row. In particular, it stores the incident energy and angle of the input particle, and the energy deposited in each scintillator layer of the target.

4.2 Stopping Cases

For the analysis of the simulation results, it was necessary to classify them. This was done by sorting the events by the layer in which they stopped: either Layer 2, Layer 3, Layer 4 or Layer 5. This is illustrated in Figure 4.1. Once the data was sorted, the energy deposited in each layer was plotted against each other layer, for that particular stopping case, i.e. Energy Deposited in Layer 2 against Energy Deposited in Layer 3, for those particles which stop in Layer 3.

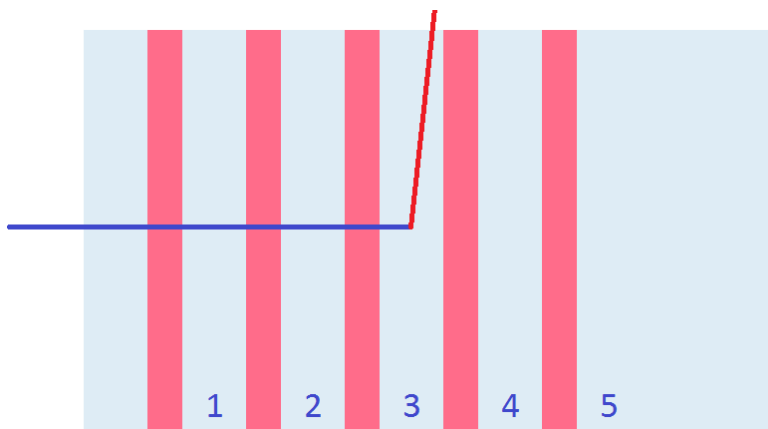


Figure 4.1: Schematic showing the numbering of the target layers. The blue line represents an input particle track, which stops in Layer 3. The red line shows the track of the scintillation photon produced.

CHAPTER 4. SIMULATION RESULTS AND ANALYSIS

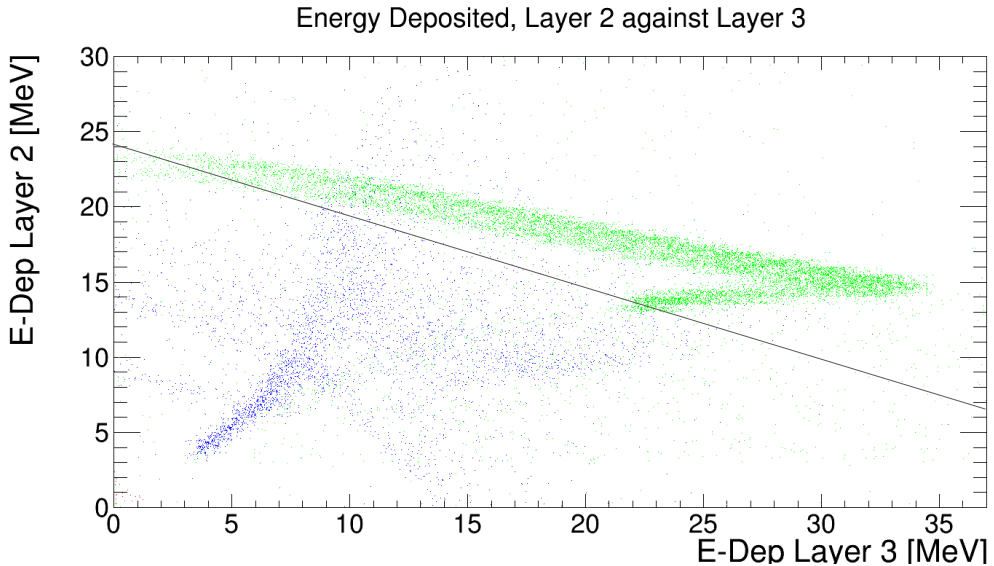


Figure 4.2: A sample plot showing the energy deposited in Layer 2 against Layer 3, for those particles which stop in Layer 3. Green denotes deuteron events, Blue denotes proton events, and Red denotes photon events. (4mm scintillator thickness). The black line shows a cut applied.

This sample plot shows the energy deposited in Layer 2 against Layer 3 for all three simulations. As you can see, each different type of particle deposits energy in a different range, making them mostly separable. In addition, both the photon events (clustered on the bottom-left) and proton events deposit energies that are mostly separate from the deuterons, and this background can be easily removed with a simple cut.

The structure visible in the deuteron signal, shown in green, is very much expected. Those particles which have deposited a lot of their energy in Layer 2 have very little left to deposit in Layer 3. Those with less energy deposited in Layer 2 have more to deposit in Layer 3. This gives rise to the top ‘arm’ of this structure. The lower ‘arm’ is from those particles which stop in Layer 3 – they have deposited some energy in Layer 2, but do not have sufficient energy to pass through Layer 3 and therefore deposit all of their remaining energy.

CHAPTER 4. SIMULATION RESULTS AND ANALYSIS

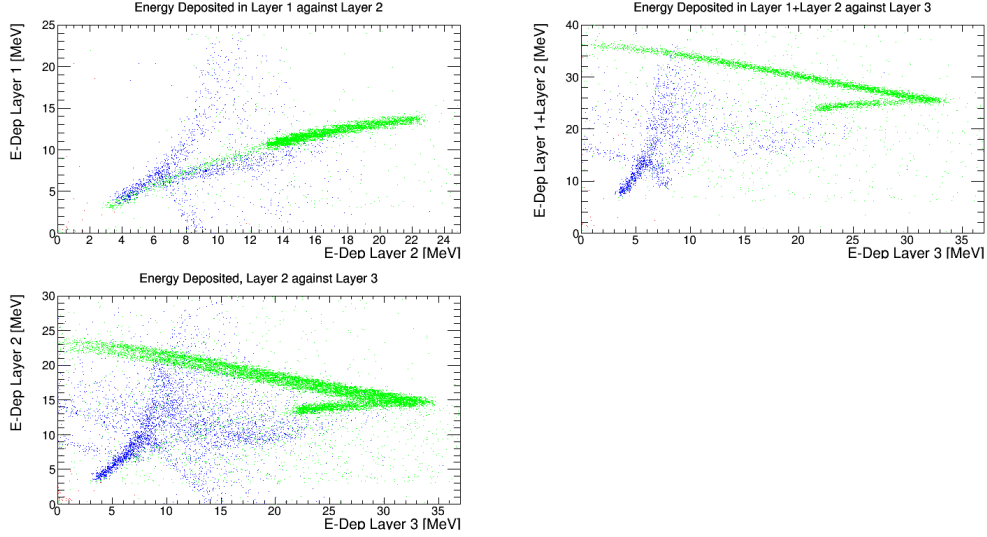


Figure 4.3: A sample stopping case - particles stopping in Layer 3 (4mm scintillator thickness).

The sample plot shown in Figure 4.2 was only one of three possible plots for those particles which stop in Layer 3 - The other possible plots for this stopping case are shown in Figure 4.3. Again, this stopping case is only one of four. For every possible plot in every possible stopping case, cuts were found which resulted in the minimum proton and photon background and the maximum deuteron signal.

Once cuts for every plot in a single stopping case were found, they were all applied to a single plot. Only those events which survived every cut could produce a deuteron signal that is distinct in energy to the background.

Once all these cuts were applied, it was possible to create a total background and total signal plot for each thickness. These were then plotted next to each other for easy comparison. These plots are shown in the next section.

4.3 Total Background and Signal

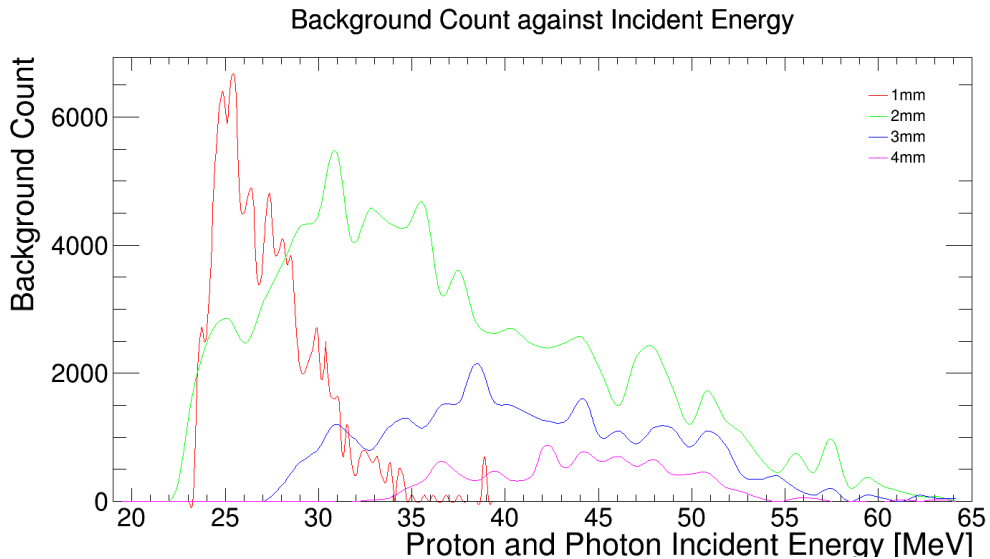


Figure 4.4: This plot shows the background surviving the cuts for each scintillator thickness, against the incident energy of the particle. The heights have been arbitrarily rescaled for easier analysis.

The total background for each thickness was plotted in Figure 4.4. The heights have been rescaled to make it easier to see any structure.

The plot shows a clear difference between the thicknesses. As the thickness increases, the minimum energy of the background also increases. This makes sense: a higher scintillator thickness results in a higher energy deposition per layer, and therefore a higher background energy.

CHAPTER 4. SIMULATION RESULTS AND ANALYSIS

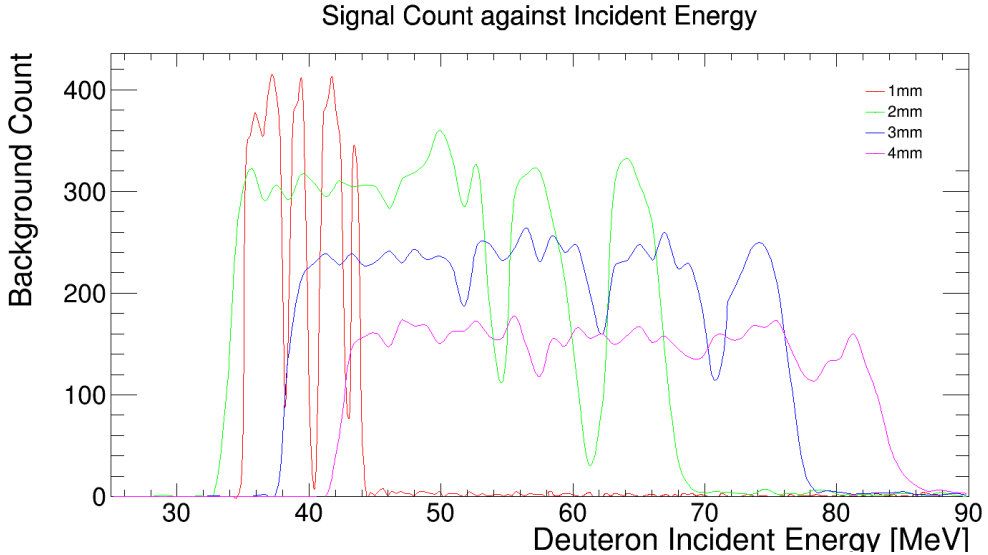


Figure 4.5: This histogram shows the deuteron signal surviving the cuts for each scintillator thickness, against the incident energy of the deuteron. The heights have been arbitrarily rescaled for easier analysis.

The plot shows, similarly to the background, that the minimum signal energy increases with scintillator thickness. No signal at all is seen below 30 MeV deuteron energy.

It is also possible to see some of the structure of the target in this plot. Especially clear in the 1mm, 2mm and 3mm plots, one can see four sharp peaks. These correspond to the different stopping cases outlined previously – particles with a high energy will stop in the higher-number layers, as they can travel through most of the target. Those with a low energy stop within the first one or two layers.

Once the total background and signal were found for each thickness, it became possible to compare them quantitatively. This is outlined in the next section.

CHAPTER 4. SIMULATION RESULTS AND ANALYSIS

4.3.1 Signal to Background

The main aim of this analysis was to obtain a signal to background ratio (SBR), as outlined in Equation 14.

$$SBR = \frac{N_D}{N_p + N_\gamma} \quad 14$$

Where N_D is the number of deuteron events which survive the cuts, N_p is the number of proton events which survive the cuts, and N_γ is the number of photon event which survive the cuts.

Each of the three different reactions have very different cross-sections: for every photo-scattered deuteron, there will be 100 quasi-free protons produced, and 1000 photon-induced reactions. Each of these simulations had the same number of events, so to compare them they had to be weighted, using the 1:100:1000 ratio for deuterons:protons:photons. The ratio for each thickness, using this weighting, is shown in Table 4.2.

| <i>Scintillator Thickness</i> | <i>Background Count</i> | <i>Signal Count</i> | <i>Signal to Background Ratio</i> |
|-----------------------------------|-----------------------------|-------------------------|---|
| 1mm | 134,500 | 8,370 | 0.062 |
| 2mm | 130,600 | 12,381 | 0.095 |
| 3mm | 66,000 | 15,576 | 0.236 |
| 4mm | 40,500 | 17,100 | 0.422 |

Table 4.2: This table shows the Signal to Background ratio for each scintillator thickness.

CHAPTER 4. SIMULATION RESULTS AND ANALYSIS

From Table 4.2, it is clear that the 4mm scintillator thickness produces the least amount of background and the most amount of signal that survives the cuts. This is equivalent to 2.38 background events for every 1 signal event.

Therefore, I would recommend that the 4mm scintillator thickness is chosen for the prototype target.

4.3.2 SBR Variation with Incident Energy

In addition to recommending the scintillator thickness, it is possible to say something about the variation of the SBR with incident energy for the 4mm case.

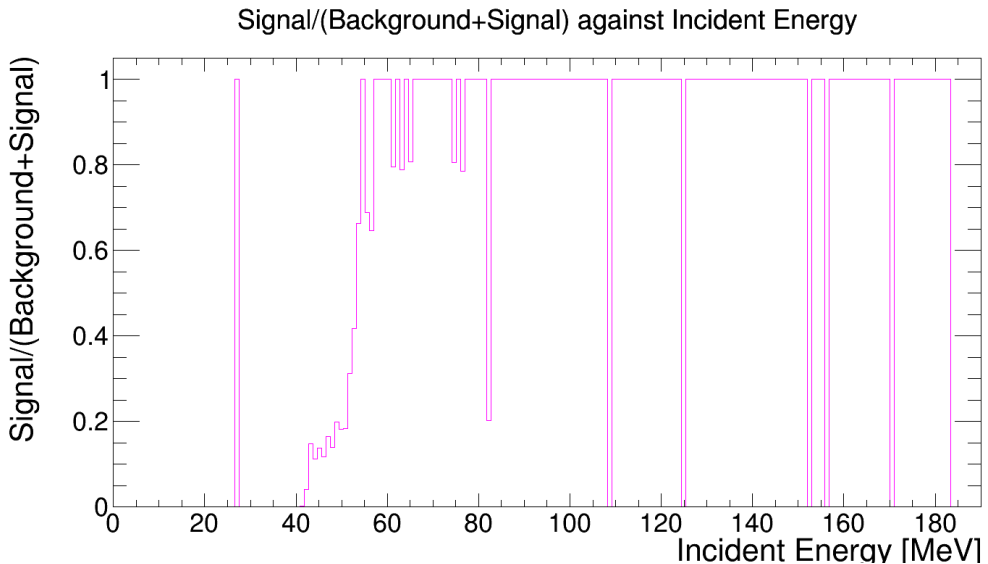


Figure 4.6: A plot of Signal/(Background + Signal) against Incident Energy for the 4mm scintillator thickness.

From Figure 4.6 it is clear that, barring a few minor outliers, the SBR is much larger above approximately 60 MeV particle energy. This may have consequences for measurement: below this energy, the background may be too large to obtain useful results, while above this energy, the deuteron signal becomes almost entirely prevalent.

Chapter 5

Conclusions

This project was successful in using Geant4 simulations to find the optimum dimensions for an active target, for use in studying the new d* dibaryon.

Specifically, it was found that a simulated cylindrical target of radius 2cm, with 5 composite layers of 1mm CD₂ deuterated plastic and 4mm vinyltoluene plastic scintillator, with four more layers of scintillator at the back and 1 layer of scintillation at the front, produced the highest Signal to Background ratio of any of the simulated thicknesses, 0.42.

This means that for any single photo-scattered deuteron, which represents the reaction products we wish to measure, there are 2.38 background events.

The variation in Signal to Background was also found to be dependent on the energy of the particle, with a minimum incident energy of 60 MeV found. Below this energy, the Signal to Background Ratio is very small, suggesting that one only use those events with an energy above this value should be used in any future analysis.

CHAPTER 6. CONCLUSION

4.4 Outlook

One of the main limitations of this project was the non-completion of the second section – the building of and experimentation on a prototype target. This would have allowed me to verify and validate the simulation results.

The opportunity for further study in this area is very clear. The next step would be to build and test the prototype according to the found dimensions.

With necessary improvements resulting from this testing of the prototype, the target would then be placed within the Crystal Ball detector and used to carry out studies on the nature of the dibaryon – specifically, whether or not the dibaryon is simply a baryonic molecule, a bound state of two baryons, or if it is a ‘genuine’ dibaryon with all six quarks in a single bag.

References

- [1] H. Clement, M. Bashkanov and T. Skorodko, “From CELSIUS to COSY: on the observation of a dibaryon resonance,” Physikalisches Institut der Universitat Tubingen, Tubingen, 2014.
- [2] S. Agostinelli et al., “Geant4 - A Simulation Toolkit,” *Nuclear Instruments and Methods*, vol. 506, pp. 250-303, 2003.
- [3] M. Gell-Mann, “A Schematic Model of Baryons and Mesons,” *Physics Letters*, vol. 8, no. 3, pp. 214-215, 1964.
- [4] H. Fritzsch and M. Gell-Mann, “Current Algebra: Quarks and What Else?,” in *Proceedings of the XVI International Conference on High Energy Physics*, Chicago, 1972.
- [5] U. Kulshreshtha, D. S. Kulshreshtha and J. P. Vary, “Hamiltonian, path integral and BRST formulations of large N scalar QCD2 on the light-front and spontaneous symmetry breaking,” *The European Physical Journal C*, pp. 174-186, 2015.
- [6] C. Gignoux, B. Silvestre-Brac and J. M. Richard, “Possibility of Stable Multiquark Baryons,” *Physics Letters B*, vol. 193, no. 2,3, pp. 323-326, 1987.
- [7] R. L. Jaffe, “Perhaps a Stable Dihyperon,” Stanford Linear Accelerator Center, Stanford, 1976.
- [8] R.A. Briceno, T.D. Cohen, S. Coito, et al., “Issues and Opportunities in Exotic Hadrons,” *Chinese Physics C*, vol. 40, no. 4, 2016.
- [9] J. Richard, “Exotic hadrons: review and perspectives,” Universite de Lyon, Villeurbanne, 2016.

- [10] F. Dyson and N.-H. Xuong, “Y=2 States in SU(6) Theory,” *Physical Review Letters*, vol. 13, 1964.
- [11] M. Gell-Mann, “Symmetries of Baryons and Mesons,” *Physical Review*, vol. 125, no. 3, 1962.
- [12] R. Bilger, H. Clement, et al., “Evidence for a dibaryon resonance in the pionic double charge exchange,” *Zeitschrift fur Physik A Hadrons and Nuclei*, vol. 343, no. 4, pp. 491-492, 1992.
- [13] T. Goldman et al., “"Inevitable" nonstrange dibaryon,” *Physical Review C*, vol. 39, no. 5, 1989.
- [14] A. Abashian, N. Booth and K. Crowe, “Possible Anomaly in Meson Production in p+d Collisions,” *Physical Review Letters*, vol. 5, no. 6-15, 1960.
- [15] M. Bashkanov, “On the Discovery of the d*(2380) Dibaryon,” Eberhard Karls Universitat Tubingen, Tubingen, 2014.
- [16] D. Watts, “The Crystal Ball programme at MAMI,” CrystalBall@MAMI collaboration, Edinburgh.
- [17] E. Brydevall, “Coupling of neutron optics and shielding using Vitess and Geant4,” Lund University, Lund, 2015.
- [18] P. Marmier and E. Sheldon, Physics of Nuclei and Particles, Academic Press, 2013.
- [19] A. Fridman, “The deuteron as target in high energy reactions,” *Fortschritte der Physik*, vol. 23, pp. 243-315, 1975.
- [20] R. Brun and F. Rademakers, “ROOT - An Object Oriented Data Analysis Framework,” in *Proceedings AIHENP'96 Workshop*, Lausanne, 1997.
- [21] C. A. Meyer; Y. Van Haarlem, “The Status of Exotic-quantum-number Mesons,” Carnegie Mellon University, Pittsburgh, 2010.

- [22] P. Adlarson et al., “Abashian-Booth-Crowe Effect in Basic Double-Pionic Fusion: A New Resonance?,” *Physical Review Letters*, vol. 106, no. 24, 2011.
- [23] F. Huang, Z. Zhang, P. Shen and W. Wang, “Is d^* a candidate of hexaquark-dominated exotic state?,” Beijing, 2015.